Heliyon 10 (2024) e35791

Contents lists available at ScienceDirect

Heliyon

journal homepage: www.cell.com/heliyon

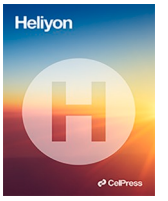

Research article

Synthesis of spinel Nickel Ferrite ($NiFe_2O_4$)/CNT electrocatalyst for ethylene glycol oxidation in alkaline medium

Fowzia S. Alamro [a], Mahmoud A. Hefnawy [b,**], Nada S. Al-Kadhi [a], Ayman M. Mostafa [c,g], Mariem M. Motawea [d], Hoda A. Ahmed [b,e], Ali S. Alshomrany [f], Shymaa S. Medany [b,*]

[a] Department of Chemistry, College of Science, Princess Nourah bint Abdulrahman University, P.O. Box 84428, Riyadh, 11671, Saudi Arabia
[b] Chemistry Department, Faculty of Science, Cairo University, 12613-Giza, Egypt
[c] Department of Physics, College of Science, Qassim University, Buraidah, 51452, Saudi Arabia
[d] Department of Chemistry, College of Science, University of Bisha, Bisha, 61922, Saudi Arabia
[e] Chemistry Department, Faculty of Science at Yanbu, Taibah University, Yanbu, 46423, Saudi Arabia
[f] Department of Physics, College of Sciences, Umm Al-Qura University, Al Taif HWY, Mecca, 24381, Saudi Arabia
[g] Spectroscopy Department, Physics Research Institute, National Research Center, Giza, 12622, Egypt

ARTICLE INFO

Keywords:
Ethylene glycol electrooxidation
Nickel ferrite
Multiwalled CNT
Nickel oxyhydroxide
EIS

ABSTRACT

Nickel-iron-based spinel oxide was prepared and supported on multi-walled carbon nanotubes to enhance the electrochemical oxidation of ethylene glycol in an alkaline medium. $NiFe_2O_4$ was prepared using facile sol-gel techniques. Then the prepared material was characterized using different bulk and surface techniques like powder X-ray diffraction (XRD), X-ray photoelectron spectroscopy (XPS), scanning electron microscope (SEM), and transmitted electron microscope (TEM). Different electrodes of $NiFe_2O_4$/CNT ratios were prepared to find out the optimum spinel oxide/CNT ratio. The activity of the metal spinel oxides composite was characterized toward ethylene glycol conversion by different electrochemical techniques like cyclic voltammetry (CV), Chronoamperometry (CA), and electrochemical impedance spectroscopy (EIS). The modified electrode reached an oxidation current of 43 mA cm^{-2} in a solution of 1.0 M ethylene glycol and 1.0 M NaOH. Furthermore, some kinetics parameters (like diffusion coefficient, and rate constant) were calculated to evaluate the catalytic performance. Additionally, the electrode showed extreme stability for long-term ethylene glycol oxidation.

1. Introduction

In today's rapidly evolving world, the need for sustainable energy resources has become paramount. As we grapple with the consequences of climate change and depleting fossil fuel reserves, it is crucial to explore and adopt alternative sources of energy that can meet our growing demands while minimizing environmental impact [1–5]. Renewable energy sources such as solar, wind, and hydropower have emerged as viable options in the pursuit of sustainability. These energy sources are abundant, widely available, and

* Corresponding author.
** Corresponding author.
E-mail addresses: maahefnawy@gmail.com, maadel@cu.edu.eg (M.A. Hefnawy), shymaasamir80@cu.edu.eg, shymaa@sci.cu.edu.eg (S.S. Medany).

https://doi.org/10.1016/j.heliyon.2024.e35791
Received 24 April 2024; Received in revised form 25 July 2024; Accepted 2 August 2024
Available online 3 August 2024

produce little to no greenhouse gas emissions. By investing in and transitioning to these renewable alternatives, we can decrease our dependency on finite fossil fuels and mitigate the harmful effects of global warming, ensuring a cleaner and healthier future for generations to come [6–9].

The electrooxidation of ethylene glycol (EG) in an alkaline medium is a fascinating area of research that holds great potential for various applications [10–12]. Because it is less poisonous than other alcohols, has a higher ignition point, is less expensive, and is not volatile, ethylene glycol (EG) has attracted a lot of attention. Additionally, EG has an energy capacity that is around 20 % greater than methanol's [13].

In recent years, there has been a growing interest in developing efficient and cost-effective materials for electrooxidation processes. One such material that has gained significant attention is nickel-based surfaces. These surfaces exhibit excellent electrocatalytic properties, making them ideal for several purposes like fuel cells, water splitting, and sensors [14–18]. The unique properties of nickel-based surfaces, such as high conductivity and corrosion resistance, make them suitable for use in harsh environments. Additionally, nickel is abundant and relatively inexpensive, further contributing to its appeal as a cost-effective material for electrooxidation. Ongoing research and development efforts aim to optimize the performance of nickel-based surfaces and explore their potential for other emerging applications in renewable energy and environmental remediation [19–25].

A remarkable chemical and thermally stable material, spinel oxides have the general structure of AB_2O_4, where A and B are metallic cations. This makes them ideal for a variety of catalytic uses. Transition metal oxides exhibiting a spinel phase are highly sought-after as anodic materials in electrochemical applications [26].

Carbon nanotubes (CNTs) have been employed as electrode modifiers in several applications. (CNTs) possess numerous characteristics that render them an outstanding nanomaterial for electrochemical applications. CNTs have been employed in the alteration of many surfaces due to their advantageous characteristics, such as improved electrical properties, elevated electric conductivity, a substantial ratio of edge planes to basal planes, a significant specific surface area, and the capacity to prevent fouling [27]. MWCNTs are commonly employed as catalyst supports in fuel cell applications such as NiCr-oxide@CNT [28], SnO_2@CNT [29], PdAg/CNT [30], Pt/MgO/CNT [31], and Pt–Sn/CNT [32].

In this work, Nickel ferrite was prepared to enhance the ethylene electrooxidation in alkaline medium. The synthesized electrocatalyst was characterized using several techniques such as XRD, XPS, SEM, and TEM. Thus, the physical mixture of CNT with nickel ferrite was prepared with different ratios. Several electrochemical studies were performed to confirm the activity of the prepared materials. Different kinetics parameters (i.e., rate constant, diffusion coefficients, and surface coverage) were calculated to find out the optimum nickel-ferrite/CNT ratio. Additionally, the electrochemical impedance spectroscopy (EIS) was utilized to find out charge transfer resistance for the modified electrodes.

2. Experimental

2.1. Preparation of nickel ferrite/CNT

A solution of sodium hydroxide with a concentration of 3.0 M was gradually combined with salt solutions containing ferric chloride ($FeCl_3.6H_2O$) at a concentration of 0.4 M and nickel chloride ($NiCl_3{\cdot}6H_2O$) at a concentration of 0.2 M. At the same time as NaOH solution was being added drop by drop, the pH of the solution was continuously checked. Over the course of the experiment, the reactants were continuously agitated with a magnetic stirrer until a pH level of more than 12 was reached. As the surfactant, a certain quantity of cetrimonium bromide (CTAB) was added to the solution. This quantity was two to three drops for a total reactive solution volume of 75 mL. After that, the liquid precipitate was heated to a reaction temperature of 80 °C and agitated for a period of 40 min. After the product had been allowed to reach room temperature, it was washed twice with distilled water and ethanol in order to eliminate any undesired contaminants and excess added. After centrifuging the sample for 15 min at a speed of two thousand revolutions per minute, it was dried at a temperature of more than 80° C for a whole night. After the substance was obtained, it was turned into a fine powder and then annealed at a temperature of 600 °C for 10 h.

Then, the prepared $NiFe_2O_4$ was mixed physically with different ratios of carbon nanotubes (i.e., 10, 25, and 40 %) to form the following electrocatalyst $NiFe_2O_4$/CNT-1, $NiFe_2O_4$/CNT-2, and $NiFe_2O_4$/CNT-3 respectively. 20 mg of electrocatalyst ($NiFe_2O_4$/CNT-1, $NiFe_2O_4$/CNT-2, and $NiFe_2O_4$/CNT-3) was suspended in 1 mL of iso-propanol and 1 mL of (5 % wt.) Nafion solutions. Then, 50 μL of catalyst ink was cast on electrode surface to prepare the final surface for electrochemical measurement.

2.2. Electrochemical measurement

The electrochemical investigations were carried out using the Autolab PGSTAT128 N equipment, employing the techniques of cyclic voltammetry, chronoamperometry, and electrochemical impedance spectroscopy. The impedance spectrum was analyzed using NOVA, an electrochemistry software developed by Metrohm Autolab in Utrecht, Netherlands. The software version used for the analysis was 2.1. A potentiostat was connected to a three-electrode cell. The experimental configuration included a reference electrode made up of Ag/AgCl/KCl (saturated) and an auxiliary electrode constructed from Pt wire. The working electrode was a modified glassy carbon (GC) electrode consisting of three different electrocatalysts: GC/$NiFe_2O_4$/CNT-1, GC/$NiFe_2O_4$/CNT-2, and GC/$NiFe_2O_4$/CNT-3. During the electrochemical impedance spectroscopy tests, the AC potential value was consistently adjusted by applying an AC voltage amplitude of 10 mV and a frequency range of 10^4 Hz–0.01 Hz. The data that was acquired was subjected to fitting using the equivalent circuits software, specifically NOVA 2.1.

The solution was first flushed using N_2 gas to remove dissolved gases. Also, electrochemical investigations were conducted under

ambient conditions.

3. Results and discussions

3.1. Structural and surface characterizations

The Powder X-Ray diffraction technique was utilized to examine the chemical composition of the produced $NiFe_2O_4$. Fig. 1a displays the XRD chart of $NiFe_2O_4$. Based on reference card ICDD No.54-0964, $NiFe_2O_4$ exhibited seven distinct peaks at precise angles, namely $2\theta = 22$, 30, 35, 36, 43, 53, 57, and 63°. The peaks observed correlate to the miller indices (111), (220), (311), (222), (400), (422), (511), and (440); respectively [33–36]. It is widely accepted that the crystal structure of $NiFe_2O_4$ is cubic, characterized by a crystal point group of m $\bar{3}$m. (see Fig. 1b). The crystal system of the $NiFe_2O_4$ was estimated using Material Studio software version 2017.

Fig. 2 demonstrates the use of X-ray photoelectron spectroscopy (XPS) to analyze the chemical structure. Nevertheless, there were two distinct peaks indicating the presence of two spin-orbit peaks of Ni 2p3/2 and Ni 2p1/2 (Fig. 2a). The detected peaks at binding energies of 854.9 and 858.4 eV can be attributed to Ni^{2+} and Ni^{3+} respectively [37–39]. The Fe 2p spectrum, depicted in Fig. 2b, exhibits two distinct peaks at 711.3 and 713.5 eV, corresponding to Fe(II) and Fe(III); respectively [40–43]. These peaks correspond to the spin–orbit peaks of Fe 2p3/2 and Fe 2p1/2, which are responsible for determining the Fe(III) oxidation state in the $NiFe_2O_4$ products. Three oxygen peaks were seen in the high-resolution spectra of the O 1s area (see Fig. 2c). These peaks manifested themselves at 530.1, 531.9, and 532.7 eV, for M(II)–O, M(III)–O and adsorbed H_2O; respectively [44–49]. The first peak, which was located at 530.1 eV, was identified as a normal M − O bond. On the other hand, the second peak, which was located at 531.9 eV, may be attributed to various defect sites, such as hydroxyls, carboxyls, or species that are intrinsic to the surface of the spinel. It is possible that the third peak, which is positioned at 532.7 eV, is connected to the H_2O that has been absorbed on the surface either physically or chemically. The spectra of C1s are shown in Fig. 2d. At binding energies of 285.14, 285.68, and 288.72 eV, the examination of the C1s spectra identified three distinct peaks. The presence of spectral peaks at 285.14 and 285.68 eV indicates the existence of a carbonaceous layer commonly seen on the surfaces of objects exposed to air [50–54]. Furthermore, the existence of metal carbonate can be deduced from the third peak, which was observed to have a binding energy of 288.72 eV.

The modified $NiFe_2O_4$/CNT-2 electrode's surface structure was investigated by scanning electron microscope (SEM). Fig. 3a displays an SEM view of the nickel ferrite surface embedded in the CNT. According to SEM, catalyst particles ranging in size from 30 nm to 60 nm were found throughout the surface. The larger particles were formed by the aggregation of the smaller structures.

The Energy Dispersive X-ray Analysis (EDAX) depicted in Fig. 3b confirms the presence of Nickel (Ni), Iron (Fe), carbon (C), and Oxygen (O) in the catalyst structure. The carbon element is due to the presence of carbon nanotubes. Otherwise, the high percentage of oxygen is due to the presence of spinel oxide, which has the chemical structure of AB_2O_4. The observed ratio of 1:2:4 between these elements is consistent with the expected composition. This finding is further corroborated by the X-ray Diffraction (XRD) analysis, which identifies $NiFe_2O_4$ as the primary phase in the catalyst structure. The catalyst's elemental surface imaging revealed a homogeneous distribution of Ni and Fe on the electrode's surface. In addition, the morphological structure of $NiFe_2O_4$ was studied using transmission electron microscopy (TEM). In Fig. 3c, the particle size is depicted as 30–60 nm. The nanoparticle loaded on CNT was investigated, as represented in Fig. 3d. Whereas the attachment of $NiFe_2O_4$ on the CNT surface for $NiFe_2O_4$/CNT-2 reflects the high activity of nickel ferrite for EG conversion.

3.2. Ethylene glycol electrochemical oxidation

The activity of the modified surface, namely, $NiFe_2O_4$/CNT-1, $NiFe_2O_4$/CNT-2, and $NiFe_2O_4$/CNT-3 electrocatalysts, were studied

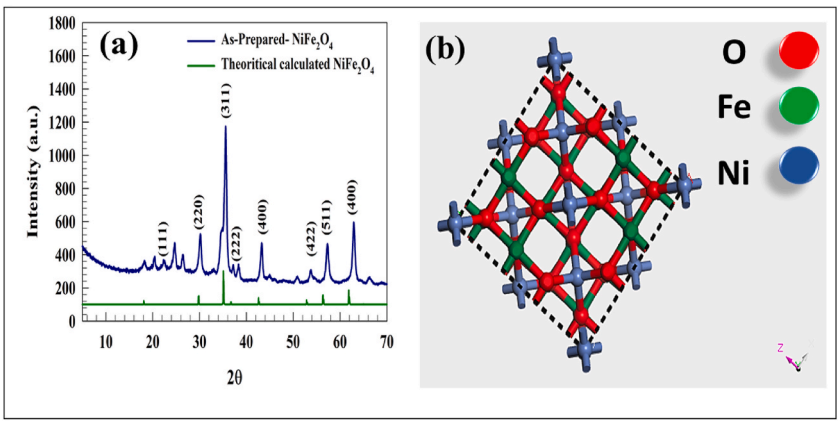

Fig. 1. a) XRD of as prepared $NiFe_2O_4$ and theoretical calculated curve. b) Crystal structure of the nickel ferrite.

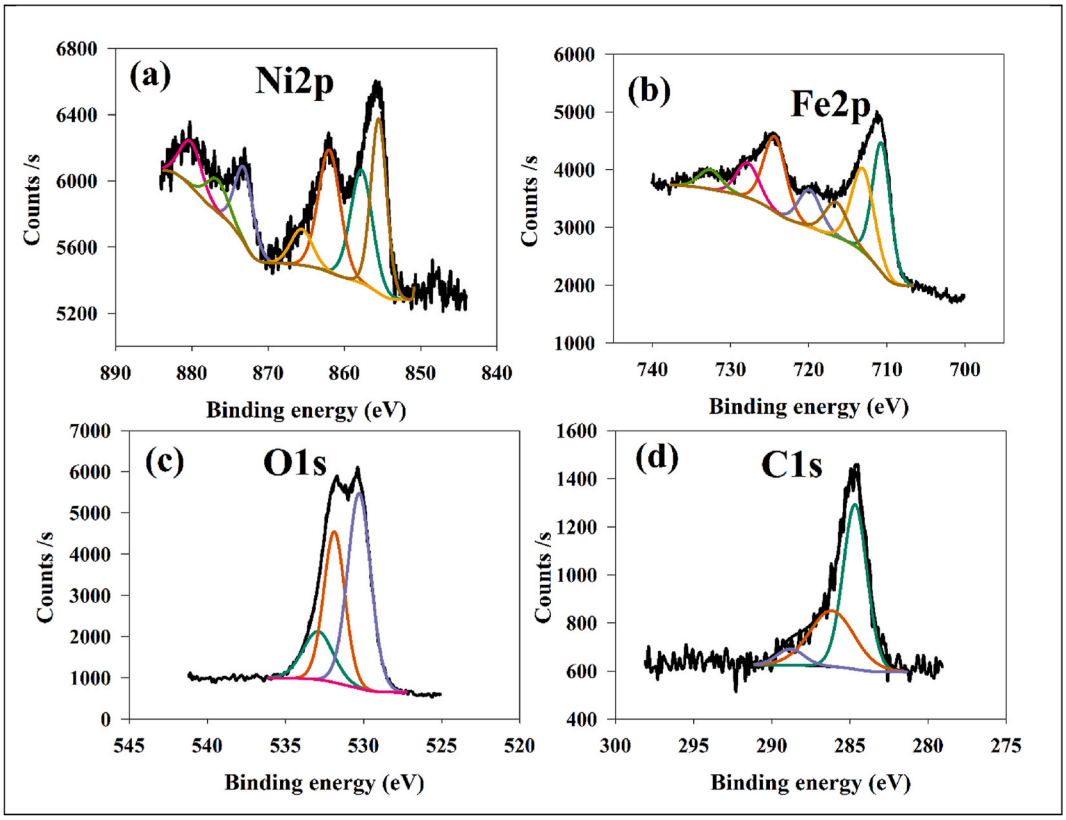

Fig. 2. XPS charts of a) Ni, **b)** Fe, **c)** O, **d)** C.

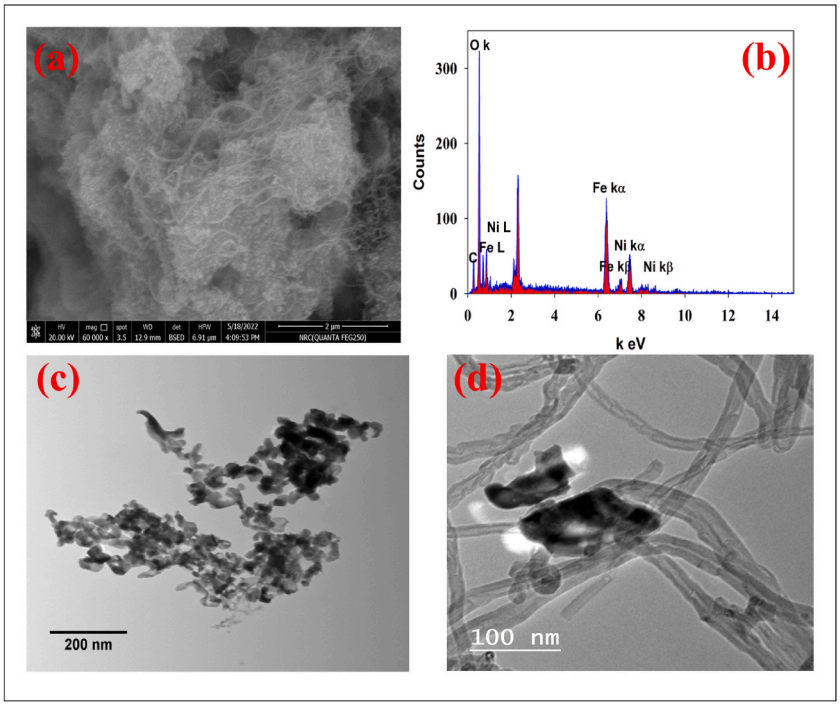

Fig. 3. a) SEM of $NiFe_2O_4$/CNT-2, b)EDAX, c) TEM of $NiFe_2O_4$, d) TEM of $NiFe_2O_4$/CNT-2.

using CVs in a solution containing 1.0 M ethylene glycol and 1.0 M NaOH. The activation of nickel-based electrodes plays a crucial role in the electrochemical oxidation of ethylene glycol. Consequently, the performance of the electrodes was improved through an activation procedure. This procedure results in the formation of a nickel-based compound that demonstrates a significant level of electrocatalytic performance, precisely known as nickel oxyhydroxide (NiOOH). The activation process was conducted using repeated CVs in NaOH for 200 cycles. The occurrence of NiOOH production results in a rise in electrical current across consecutive cycles. As the quantity of potential sweeps rises, the thickness of the NiOOH layer proportionally increases. The presence of OH^- ions is responsible for facilitating the conversion rate between $Ni(OH)_2$ and $NiOOH$, as described by the following equation **no.1** [55,56]:

$$6\,Ni(OH)_2 + 6OH^- \leftrightarrow 6\,NiOOH + 6H_2O + 6\,e^- \tag{1}$$

The NiOOH species produced is mostly utilized for the electrochemical oxidation of ethylene glycol, as determined by equation **no. 2** [57,58]:

$$(CH_2OH)_2 + 10\,OH^- \leftrightarrow 2CO_2 + 8H_2O + 10e^- \tag{2}$$

The CVs of the modified $NiFe_2O_4$/CNT in a 1.0 M NaOH solution are illustrated in Fig. 4a. The conversion of $Ni(OH)_2$ and NiOOH exhibits a single redox peak within the potential range of 0.3–0.45 V. Fig. 4b illustrates the process of EG oxidation. Hence, the presence of prominent oxidation peaks at a potential of less than 0.45 V can be attributed to the transformation of EG. Nevertheless, the $NiFe_2O_4$/CNT-2 sample exhibited significantly higher activity in comparison to the other modified $NiFe_2O_4$/CNT sample. The use of carbon nanotubes has the potential to augment the efficacy of EG electrochemical oxidation in an alkaline environment. The increased ability of CNT to enhance the electrical conductivity of the electrode surface along with computability between catalyst and electrode surface. Also, surface area and improved mechanical and chemical durability of CNT-based samples may account for the greater activity seen in EG electrochemical oxidation.

A study was conducted to assess the electroactive surface area of each electrode by studying its correlation with surface coverage. The research examines the cyclic voltammetry of different modified electrodes, specifically $NiFe_2O_4$/CNT-1, $NiFe_2O_4$/CNT-2, and $NiFe_2O_4$/CNT-3, in a 1.0 M NaOH solution at different sweep rates (see Fig. 5a-c). The depicted diagram demonstrates that the oxidation peaks exhibited a shift towards a more positive value as the sweep rate was increased. For all electrocatalysts, the reduction peaks exhibited a tendency towards more negative values. The observed outcome can be ascribed to the augmentation of active sites on the surface of the electrocatalyst by the amplification of the scan rate. Fig. 5d displays the linear relationships between the scan rate and the oxidation and reduction peaks of the electrocatalyst. Hence, equation no.3 is employed to determine the extent of active site coverage on the surface of each electrocatalyst [59]:

$$I_p = \left(\frac{n^2F^2}{4RT}\right) \upsilon\, A\Gamma^* \tag{3}$$

The equation contains the following variables: R denotes the universal gas constant, T represents the solution temperature. υ indicates the sweep rate of cyclic voltammetry, measured in mV s^{-1}. A represents the electrode surface area, which is 0.0707 cm^2. Lastly, Γ^* represents the surface coverage of redox species, measured in mol cm^2. The process of obtaining the value of Γ * involved calculating the slope of the linear relationship between I_p and υ. the surface coverages provide are 4.17×10^{-9}, 3.81×10^{-8}, and 6.54×10^{-11} mol cm^2 for $NiFe_2O_4$/CNT-1, $NiFe_2O_4$/CNT-2, and $NiFe_2O_4$/CNT-3; respectively.

The study also assessed the electrochemical response of the $NiFe_2O_4$/CNT-1, $NiFe_2O_4$/CNT-2, and $NiFe_2O_4$/CNT-3 modified electrodes to variations in fuel concentration. The investigation of the impact of different ethylene glycol concentrations was conducted by employing a scan rate of 20 mV s^{-1} in a solution containing 1.0 M NaOH, as depicted in Fig. 6a–c. The magnitude of the anodic peak current exhibited a positive correlation with the content of ethylene glycol. Fig. 6d illustrates the correlation between the concentration of ethylene glycol and the anodic peak current. Based on the results of the investigation, it can be concluded that the suggested composite exhibits potential as a viable alternative to ethanol electrooxidation due to its adaptability in effectively functioning across different ethylene glycol concentrations. Table 1 presents a comparison of the anodic current of the modified $NiFe_2O_4$/

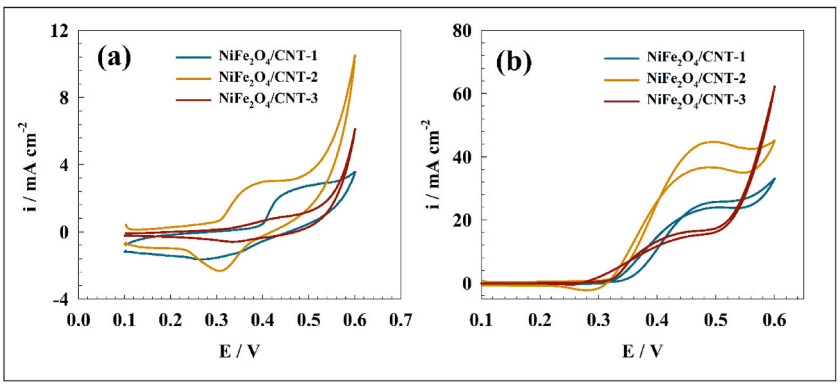

Fig. 4. CVs of modified $NiFe_2O_4$/CNT-1, $NiFe_2O_4$/CNT-2, and $NiFe_2O_4$/CNT-3 in solution of EG and NaOH.

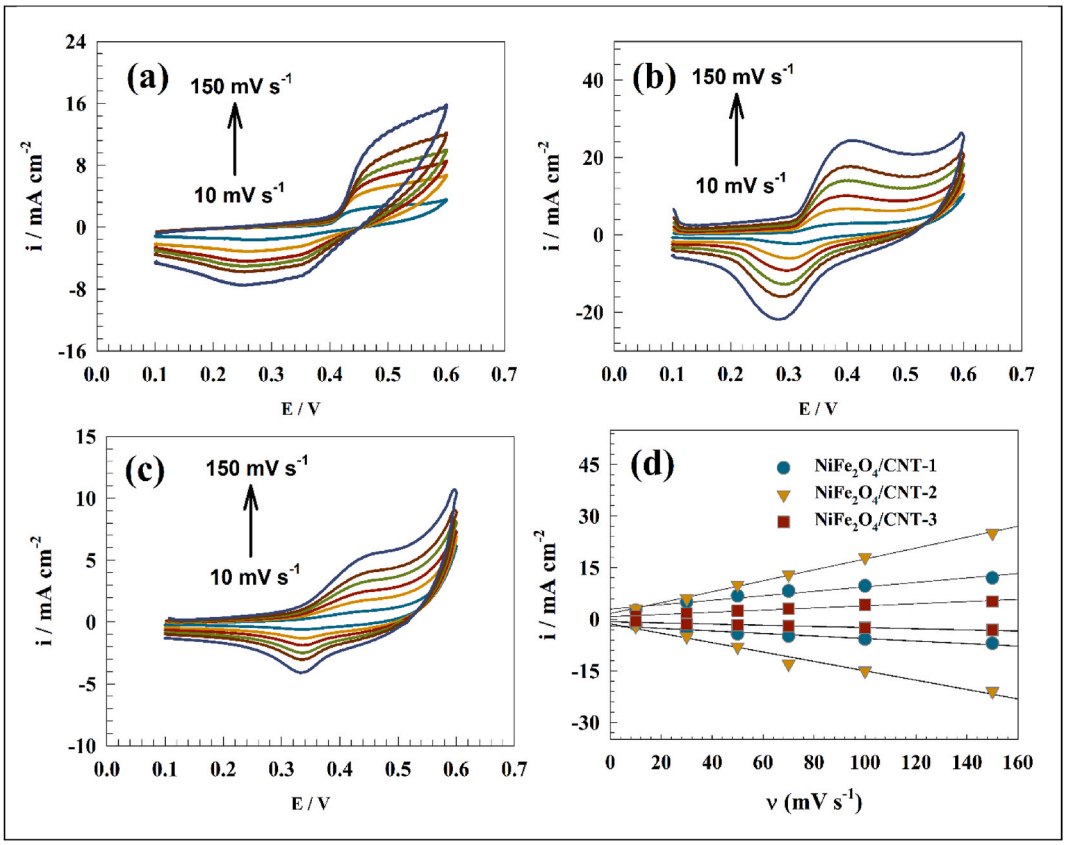

Fig. 5. CVs of (a) $NiFe_2O_4$/CNT-1, (b) $NiFe_2O_4$/CNT-2, and (c) $NiFe_2O_4$/CNT-3 in 1.0 M NaOH. d) Relation between anodic or cathodic current and the sweep rate.

CNT-2 composite with other nickel-based electrodes documented in the existing literature.

The study utilized chronoamperometry to investigate the extended endurance of the ethylene glycol electrochemical oxidation surface (refer to Fig. 7a). Chronoamperometry experiments were conducted on the surfaces of $NiFe_2O_4$@CNT-1, $NiFe_2O_4$/CNT-2, and $NiFe_2O_4$/CNT-3 in a solution containing 1.0 M ethylene glycol and 1.0 M NaOH. The experiments were carried out at a fixed potential of 0.45 V. After 10 h, the oxidation current density of the electrodes fell by 9 %, 6 %, and 15 % for $NiFe_2O_4$/CNT-1, $NiFe_2O_4$/CNT-2, and $NiFe_2O_4$/CNT-3; respectively. The current decline is attributed to the mechanical corrosion of the electrocatalyst surface, the buildup of partially oxidized EG, and the formation of metal carbonate resulting from the binding of the generated carbon monoxide [65]. Nevertheless, minor variations in the anodic current indicate that the electrodes demonstrate enhanced durability and stability to the electrochemical transformation of ethylene glycol over long time.

The rate constant (k) and diffusion coefficient (D) were estimated using the constant potential chronoamperometry method. The constant potential chronoamperometry is carried out for modified $NiFe_2O_4$/CNT-2 surface in the presence of various fuel concentrations (range from 0.05 to 1.0 M) in 1.0 M NaOH at potential of 0.45 V (see Fig. 7b). In addition, the diffusion coefficient was estimated for $NiFe_2O_4$/CNT-2 at different concentrations of EG using Cottrell equation (Equation no. 4). Whereas the D was calculated by plotting relation between anodic current and $t^{-0.5}$ (see Fig. 7c) [66,67]:

$$i = \frac{nFA\, C\sqrt{D}}{\sqrt{\pi t}} \tag{4}$$

In the oxidation process, the variables are as follows: n: number of electron, F: Faraday constant, A is electrode's area, C_o represents the concentration of EG, D represents the diffusion coefficient, and t represents experiment's time. The diffusion coefficient was determined by analyzing the correlation between the oxidation current and the square root of time ($t^{1/2}$), as depicted in Fig. 7c. Table 2 presented the D values for different concentrations of EG. The ethylene glycol molecule displayed a reduced diffusion coefficient due to the robust intermolecular interaction, particularly the hydrogen bond, between the fuel and the solvent.

The constant potential chronoamperometry method is used to determine the rate constant (ks) of modified surfaces at different concentrations of EG, as indicated in Table 2. Regarding to equation **No. 5** [68]:

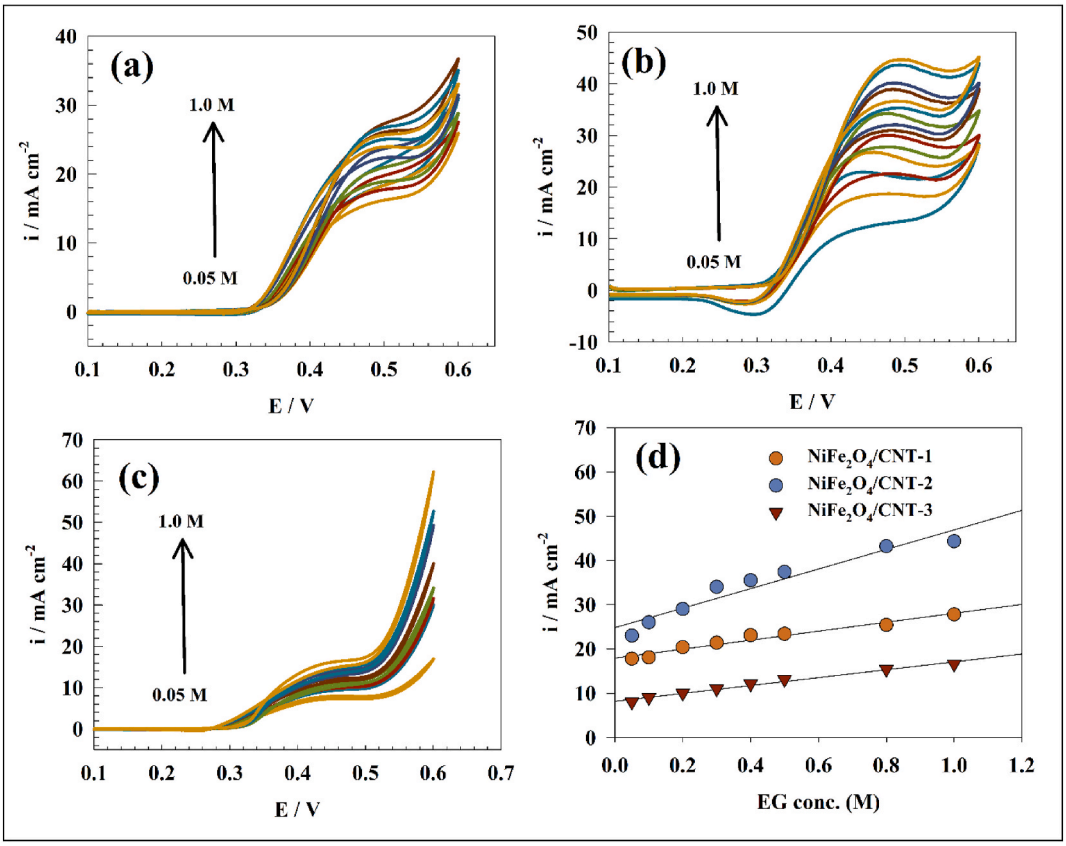

Fig. 6. CVs of (a) $NiFe_2O_4$/CNT-1, (b) $NiFe_2O_4$/CNT-2, and (c) $NiFe_2O_4$/CNT-3 in a solution of 1 M NaOH containing different EG concentration. d) Relation between anodic current and EG concentration.

Table 1
Comparison between modified $NiFe_2O_4$/CNT-2 electrode with others reported in literature for EG oxidation.

Surface	EG (M)	NaOH (M)	Sweep rate (mV s^{-1})	current density (mA cm^{-2})	Reference
$NiFe_2O_4$/CNT-2	1.0	1.0	20	43	This work
$NiMn_2O_4$@Carbon felt	1.0	1.0	20	24	[11]
$NiCo_2O_4$@Chitosan	1.0	1.0	20	42	[60]
IN738 Superalloy	1.0	1.0	20	17	[61]
Pd-(NiZn)–C	5.0	2.0	50	84.2	[62]
PdNiP	1.0	1.0	20	31.3	[63]
Sulfonate-MWCNT- PdNi	0.5	1.0	50	35.3	[64]

$$\frac{i_c}{i_d} = \pi^{0.5} \left(k_s\, C_o\, t\right)^{0.5} \tag{5}$$

The equation contains the following variables: The symbol "Ic" denotes the catalytic anodic current (A), "I_d": electrode current in the absence of fuel, "C": EG concentration (M), "k": the rate constant (M^{-1} s^{-1}), and "t": time (s).

In order to estimate the rate constant, the slope of the connection between I_C/I_L and $t^{1/2}$ was calculated, as depicted in Fig. 7d. The analysis of the data reported in Table 2 revealed that the rate constant displayed a wide range of values across various concentrations. However, the diffusion coefficient plays important role in electrooxidation of ethylene glycol. Thus, the high interaction between EG molecules under electric field has an influence on rate constant.

EIS spectroscopy was utilized to examine the influence of composite modification on the electrochemical characteristics of EG electrooxidation. Fig. 8a presents Nyquist plots of the electrodes modified with $NiFe_2O_4$/CNT-1, $NiFe_2O_4$/CNT-2, and $NiFe_2O_4$/CNT-3 in 1.0 M EG and 1.0 M NaOH at AC potential equal +0.450 V. Nevertheless, the impedance value aligns with the data found in the CV analysis. Additionally, it is worth noting that the electrode with the highest activity, $NiFe_2O_4$/CNT-2, demonstrates the lowest charge transfer resistance (R2). Furthermore, the high R2 value of $NiFe_2O_4$/CNT-3 corresponded to the lowest observed activity. Table 3 presents the values of the fitting parameters for Nyquist data. These parameters include the solution resistance (Rs), outer layer

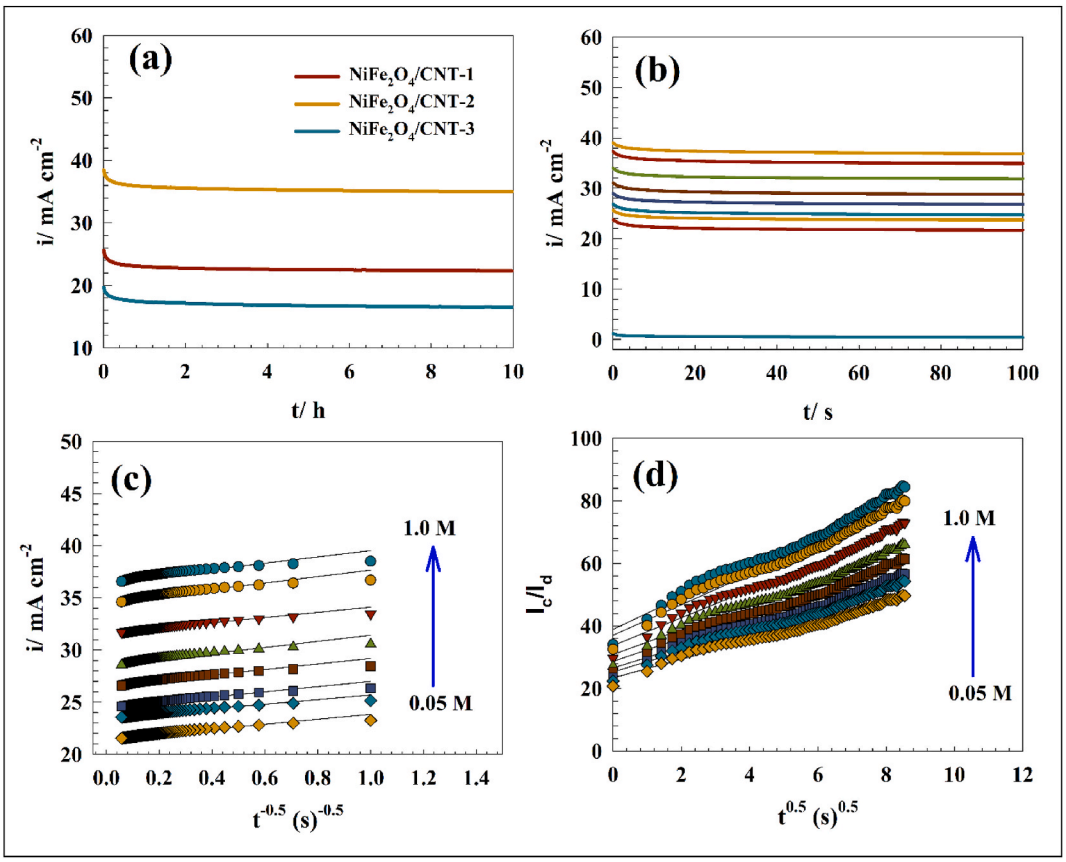

Fig. 7. a) Long-term stability of different $NiFe_2O_4$/CNT-1, $NiFe_2O_4$/CNT-2, and $NiFe_2O_4$/CNT-3 electrodes, b) chronoamperometry for $NiFe_2O_4$/CNT-2 at different EG concentrations. c) Linear relation between andic current versus $t^{-0.5}$. d) Linear relation between I_C/I_d versus $t^{0.5}$.

Table 2
Representation of D, and k for $NiFe_2O_4$/CNT-2 at different EG concentrations.

EG Conc. (M)	0.05	0.1	0.2	0.3	0.4	0.5	0.8	1.0
$D \times 10^{-9}$ ($cm^2\ s^{-1}$)	19	14	8.2	4.92	2.4	1.62	0.84	0.42
k_s ($mol^{-1}\ L\ s^{-1}$)	13	8.56	8.43	5.25	4.53	4.02	3.85	2.18

resistance (R1), outer layer capacitance (C1), inner layer resistance (R2), and inner layer capacitance (C2), all of which are connected to the inner layer in the circuit. Moreover, the electrochemical behavior is influenced synergistically by the fluctuation in fuel concentration. In contrast, an electrochemical impedance spectroscopy (EIS) analysis was conducted on the electrode ($NiFe_2O_4$/CNT-2) with the highest electrochemical oxidation value for EG in a solution containing 1.0 M NaOH and a potential of +0.45 V. Nyquist plots for different EG concentrations, ranging from 0.05 to 1.0 M, were shown in Fig. 8b. The data for the fitted equivalent electric circuit was shown in Table 4. As the EG content increases, the surface's resistance related to charge transfer decreases due to the electrochemical oxidation process. Nevertheless, the rise in fuel concentrations results in a reduction in the charge transfer resistance and impedance of the electrode. This is attributed to the heightened resultant current of the ethylene glycol (EG) oxidation process.

4. Conclusions

The study of the activity of nickel iron functionalized carbon nanotube was performed in the alkaline medium. Thus, synergistic effect between nickel iron and carbon nanotube was observed as the presence of CNT enhanced the performance of the spinel oxide for EG electrooxidation. The reason for enhancement of oxidation power is regarding the higher electrical conductivity of CNT which promotes the charge transfer step. Also, the high surface area of CNT could enhance the adsorption step. The ratio of NiF_2O_4: CNT (75:25 %) showed the highest activity as the lower nickel content led to decrease the available active sites for oxidation. $NiFe_2O_4$/CNT-2 has the highest surface coverage among the others (3.81×10^{-8} mol cm^2). Additionally, the modified electrode showed high activity through EG concentrations (0.05–1.0 M). The electrode showed low diffusion coefficient due to the interaction between EG with each

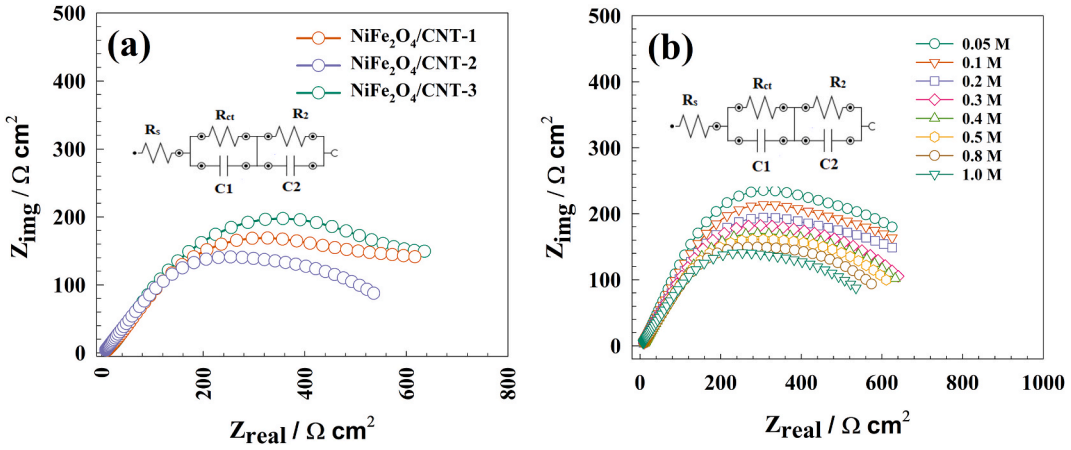

Fig. 8. a) Nyquist plot for different modified electrode $NiFe_2O_4$/CNT-1, $NiFe_2O_4$/CNT-2, and $NiFe_2O_4$/CNT-3, b) Nyquist plot for modified $NiFe_2O_4$/CNT-2 at various EG concentrations.

Table 3
Nyquist fitting parameters for different electrode surface.

Electrode	R_s (Ω cm^2)	R_1 (Ω cm^2)	C_1 (F)	R_2 (Ω cm^2)	C_2(F)
$NiFe_2O_4$/CNT-1	14.3	23.4	0.0004354	624	0.000778
$NiFe_2O_4$/CNT-2	15.7	21.7	0.0007248	562	0.000954
$NiFe_2O_4$/CNT-3	14.9	27.1	0.0001854	662	0.000359

Table 4
Nyquist fitting parameters for different concentration for $NiFe_2O_4$/CNT-2 electrode.

EG conc. (M)	R_s (Ω cm^2)	R_1 (Ω cm^2)	C_1 (F)	R_2 (Ω cm^2)	C_2 (F)
0.05	15.1	26.4	0.0004182	658	0.000471
0.1	14.3	25.9	0.0004281	649	0.000484
0.2	16.5	25.64	0.0004357	637	0.000506
0.3	12.5	24.9	0.0004783	634	0.000727
0.4	14.6	23.8	0.0004851	615	0.000762
0.5	13.9	24.6	0.0005019	603	0.000807
0.8	14.8	23.1	0.0006187	589	0.000841
1.0	15.7	21.7	0.0007248	562	0.000954

other and solvent molecules (by strong hydrogen bond). The high percentage of CNT in $NiFe_2O_4$/CNT-3 sample showed lower activity due to the lower available nickel active sites in the electrode surface.

Funding

This research was funded by to "Princess Nourah bint Abdulrahman University Researchers Supporting Project number (PNURSP2024R107), Princess Nourah bint Abdulrahman University, Riyadh, Saudi Arabia".

Data availability statement

The datasets used and analyzed during the current study are available from the corresponding author upon reasonable request.

CRediT authorship contribution statement

Fowzia S. Alamro: Writing – review & editing, Resources, Project administration, Funding acquisition. **Mahmoud A. Hefnawy:** Writing – review & editing, Writing – original draft, Visualization, Validation, Software, Resources, Methodology, Investigation, Formal analysis, Data curation, Conceptualization. **Nada S. Al-Kadhi:** Writing – review & editing, Project administration, Methodology, Funding acquisition. **Ayman M. Mostafa:** Writing – review & editing, Resources, Project administration, Funding acquisition. **Mariem M. Motawea:** Writing – review & editing, Resources, Project administration, Funding acquisition. **Hoda A. Ahmed:** Writing – review & editing, Project administration, Investigation, Funding acquisition. **Ali S. Alshomrany:** Resources, Project administration,

Investigation, Funding acquisition. **Shymaa S. Medany:** Writing – review & editing, Writing – original draft, Visualization, Validation, Software, Resources, Methodology, Investigation, Formal analysis, Data curation, Conceptualization.

Declaration of competing interest

The authors declare that there is no conflict of interest regarding the publication of this paper.

Acknowledgments

The authors extend their sincere appreciation to "Princess Nourah bint Abdulrahman University Researchers Supporting Project number (PNURSP2024R107), Princess Nourah bint Abdulrahman University, Riyadh, Saudi Arabia".

The authors are thankful to the Deanship of Graduate Studies and Scientific Research at University of Bisha for supporting this work through the Fast-Track Research Support Program.

References

[1] J. Friedrichs, The Future Is Not what it Used to Be: Climate Change and Energy Scarcity, MIT Press, 2013.
[2] N.H. Afgan, D. Al Gobaisi, M.G. Carvalho, M. Cumo, Sustainable energy development, Renew. Sustain. Energy Rev. 2 (1998) 235–286.
[3] M. Dhali, S. Hassan, U. Subramaniam, Comparative analysis of oil and gas legal frameworks in Bangladesh and Nigeria: a pathway towards achieving sustainable energy through policy, Sustainability 15 (2023) 15228.
[4] H. Gamal, A.M. Elshahawy, S.S. Medany, M.A. Hefnawy, M.S. Shalaby, Recent advances of vanadium oxides and their derivatives in supercapacitor applications: a comprehensive review, J. Energy Storage 76 (2024) 109788, https://doi.org/10.1016/j.est.2023.109788.
[5] A.M. Fekry, I. V Filippova, S.S. Medany, S.A. Abdel-Gawad, L.O. Filippov, Use of a natural rock material as a precursor to inhibit corrosion of Ti alloy in an aggressive phosphoric acid medium, Sci. Rep. 14 (2024) 9807, https://doi.org/10.1038/s41598-024-60403-0.
[6] X. Li, Z. Chen, X. Fan, Z. Cheng, Hydropower development situation and prospects in China, Renew. Sustain. Energy Rev. 82 (2018) 232–239.
[7] E.F. Moran, M.C. Lopez, N. Moore, N. Müller, D.W. Hyndman, Sustainable hydropower in the 21st century, Proc. Natl. Acad. Sci. 115 (2018) 11891–11898.
[8] C.G. Granqvist, Solar energy materials, Adv. Mater. 15 (2003) 1789–1803.
[9] N. Kannan, D. Vakeesan, Solar energy for future world:-A review, Renew. Sustain. Energy Rev. 62 (2016) 1092–1105.
[10] F.S. Alamro, S.S. Medany, N.S. Al-Kadhi, A.M. Mostafa, W.F. Zaher, H.A. Ahmed, M.A. Hefnawy, Controllable synthesis of Fe2O3/nickel cobaltite electrocatalyst to enhance oxidation of small molecules, Catalysts 14 (2024), https://doi.org/10.3390/catal14050329.
[11] S.S. Medany, M.A. Hefnawy, S.M. Kamal, High-performance spinel NiMn2O4 supported carbon felt for effective electrochemical conversion of ethylene glycol and hydrogen evolution applications, Sci. Rep. 14 (2024) 471, https://doi.org/10.1038/s41598-023-50950-3.
[12] X.-Y. Ma, H.-Z. Ma, S.-H. He, Y. Zhang, Y.-N. Yi, Y.-Y. Yang, The electrocatalytic activity and selectivity of ethylene glycol oxidation into value-added chemicals at iron-group electrodes in alkaline media, Mater. Today Phys. 37 (2023) 101191, https://doi.org/10.1016/j.mtphys.2023.101191.
[13] V. Livshits, M. Philosoph, E. Peled, Direct ethylene glycol fuel-cell stack—study of oxidation intermediate products, J. Power Sources 178 (2008) 687–691, https://doi.org/10.1016/j.jpowsour.2007.07.054.
[14] A.S. Eliwa, M.A. Hefnawy, S.S. Medany, R.G. Deghadi, W.M. Hosny, G.G. Mohamed, Ultrasonic-assisted synthesis of nickel metal-organic framework for efficient urea removal and water splitting applications, Synth. Met. 294 (2023) 117309, https://doi.org/10.1016/j.synthmet.2023.117309.
[15] F.S. Alamro, M.A. Hefnawy, S.S. Nafee, N.S. Al-Kadhi, R.A. Pashameah, H.A. Ahmed, S.S. Medany, Chitosan supports boosting NiCo2O4 for catalyzed urea electrochemical removal application, Polymers 15 (2023), https://doi.org/10.3390/polym15143058.
[16] N.S. Al-Kadhi, M.A. Hefnawy, F.S. Alamro, R.A. Pashameah, H.A. Ahmed, S.S. Medany, Polyaniline-supported nickel oxide flower for efficient nitrite electrochemical detection in water, Polymers 15 (2023), https://doi.org/10.3390/polym15071804.
[17] M.A. Bhatti, K.F. Almaani, A.A. Shah, A. Tahira, A.D. Chandio, A.Q. Mugheri, A. liaquat Bhatti, B. Waryani, S.S. Medany, A. Nafady, Z.H. Ibupoto, Low temperature aqueous chemical growth method for the doping of W into ZnO nanostructures and their photocatalytic role in the degradration of methylene blue, J. Clust. Sci. 33 (2022) 1445–1456, https://doi.org/10.1007/s10876-021-02069-6.
[18] J. Kumar, R.A. Soomro, R.R. Neiber, N. Ahmed, S.S. Medany, M.D. Albaqami, A. Nafady, Ni nanoparticles embedded Ti3C2Tx-MXene nanoarchitectures for electrochemical sensing of methylmalonic acid, Biosensors 12 (2022), https://doi.org/10.3390/bios12040231.
[19] L. Huo, C. Jin, K. Jiang, Q. Bao, Z. Hu, J. Chu, Applications of nickel-based electrocatalysts for hydrogen evolution reaction, Adv. Energy Sustain. Res. 3 (2022) 2100189.
[20] Z. Angeles-Olvera, A. Crespo-Yapur, O. Rodríguez, J.L. Cholula-Díaz, L.M. Martínez, M. Videa, Nickel-based electrocatalysts for water electrolysis, Energies 15 (2022) 1609.
[21] M. Gong, D.-Y. Wang, C.-C. Chen, B.-J. Hwang, H. Dai, A mini review on nickel-based electrocatalysts for alkaline hydrogen evolution reaction, Nano Res. 9 (2016) 28–46.
[22] X. Li, F.C. Walsh, D. Pletcher, Nickel based electrocatalysts for oxygen evolution in high current density, alkaline water electrolysers, Phys. Chem. Chem. Phys. 13 (2011) 1162–1167.
[23] X. Liu, X. Wang, X. Yuan, W. Dong, F. Huang, Rational composition and structural design of in situ grown nickel-based electrocatalysts for efficient water electrolysis, J. Mater. Chem. A. 4 (2016) 167–172.
[24] V. Vij, S. Sultan, A.M. Harzandi, A. Meena, J.N. Tiwari, W.-G. Lee, T. Yoon, K.S. Kim, Nickel-based electrocatalysts for energy-related applications: oxygen reduction, oxygen evolution, and hydrogen evolution reactions, ACS Catal. 7 (2017) 7196–7225.
[25] J. Li, L. Li, X. Ma, X. Han, C. Xing, X. Qi, R. He, J. Arbiol, H. Pan, J. Zhao, Selective ethylene glycol oxidation to formate on nickel selenide with simultaneous evolution of hydrogen, Adv. Sci. (2023) 2300841.
[26] S. Zhang, S. Liu, X. Zhu, Y. Yang, W. Hu, H. Zhao, R. Qu, C. Zheng, X. Gao, Low temperature catalytic oxidation of propane over cobalt-cerium spinel oxides catalysts, Appl. Surf. Sci. 479 (2019) 1132–1140.
[27] N. Gupta, S.M. Gupta, S.K. Sharma, Carbon nanotubes: synthesis, properties and engineering applications, Carbon Lett 29 (2019) 419–447.
[28] Q. Gan, B. Wang, J. Chen, J. Tian, T.T. Isimjan, X. Yang, Exploring the effect of Ni/Cr contents on the sheet-like NiCr-oxide-decorated CNT composites as highly active and stable catalysts for urea electrooxidation, Clean Energy 4 (2020) 58–66.
[29] X. Zhang, H. Zhu, Z. Guo, Y. Wei, F. Wang, Design and preparation of CNT@ SnO2 core-shell composites with thin shell and its application for ethanol oxidation, Int. J. Hydrogen Energy 35 (2010) 8841–8847.
[30] J. Qi, N. Benipal, C. Liang, W. Li, PdAg/CNT catalyzed alcohol oxidation reaction for high-performance anion exchange membrane direct alcohol fuel cell (alcohol= methanol, ethanol, ethylene glycol and glycerol), Appl. Catal. B Environ. 199 (2016) 494–503.
[31] B. Liu, J.H. Chen, C.H. Xiao, K.Z. Cui, L. Yang, H.L. Pang, Y.F. Kuang, Preparation of Pt/MgO/CNT hybrid catalysts and their electrocatalytic properties for ethanol electrooxidation, Energy Fuel. 21 (2007) 1365–1369.
[32] L.A. Romero-Cano, G. Rosado-Ortiz, A.M. Valenzuela-Muñiz, L.C. Ordóñez, R. Gauvin, Y.V. Gómez, Solvent effect in the synthesis of nanostructured Pt–Sn/CNT as electrocatalysts for the electrooxidation of ethanol, Int. J. Hydrogen Energy 44 (2019) 12430–12438.

[33] A. Al-Hunaiti, A. Ghazzy, N. Sweidan, Q. Mohaidat, I. Bsoul, S. Mahmood, T. Hussein, Nano-magnetic NiFe2O4 and its photocatalytic oxidation of vanillyl alcohol—synthesis, characterization, and application in the valorization of lignin, Nanomaterials 11 (2021), https://doi.org/10.3390/nano11041010.

[34] C. Jia, Y. Zhang, Q. Kong, Q. Wang, G. Chen, H. Guam, C. Dong, Soft-template synthesis of mesoporous NiFe2O4 for highly sensitive acetone detection, J. Mater. Sci. Mater. Electron. 31 (2020) 6000–6007.

[35] F.S. Alamro, S.S. Medany, N.S. Al-Kadhi, H.A. Ahmed, M.A. Hefnawy, Modified NiFe2O4-supported graphene oxide for effective urea electrochemical oxidation and water splitting applications, Molecules 29 (2024) 1215.

[36] A.H. Bashal, M.A. Hefnawy, H.A. Ahmed, M.A. El-Atawy, R.A. Pashameah, S.S. Medany, Green Synthesis of NiFe2O4 Nano-Spinel Oxide-Decorated Carbon Nanotubes for Efficient Capacitive Performance—Effect of Electrolyte Concentration, Nanomaterials, vol. 13, 2023, https://doi.org/10.3390/nano13192643.

[37] M.B. Islam, M. Yanagida, Y. Shirai, Y. Nabetani, K. Miyano, NiOx hole transport layer for perovskite solar cells with improved stability and reproducibility, ACS Omega 2 (2017) 2291–2299, https://doi.org/10.1021/acsomega.7b00538.

[38] Z. Fu, J. Hu, W. Hu, S. Yang, Y. Luo, Quantitative analysis of Ni2+/Ni3+ in Li[NixMnyCoz]O2 cathode materials: non-linear least-squares fitting of XPS spectra, Appl. Surf. Sci. 441 (2018) 1048–1056, https://doi.org/10.1016/j.apsusc.2018.02.114.

[39] L. Qiao, X. Bi, Direct observation of Ni3+ and Ni2+ in correlated LaNiO3−δ films, Europhys, Lett. 93 (2011) 57002, https://doi.org/10.1209/0295-5075/93/57002.

[40] A.P. Grosvenor, B.A. Kobe, M.C. Biesinger, N.S. McIntyre, Investigation of multiplet splitting of Fe 2p XPS spectra and bonding in iron compounds, Surf. Interface Anal. An Int. J. Devoted to Dev. Appl. Tech. Anal. Surfaces, Interfaces Thin Film 36 (2004) 1564–1574.

[41] H.W. Nesbitt, M. Scaini, H. Hochst, G.M. Bancroft, A.G. Schaufuss, R. Szargan, Synchrotron XPS evidence for Fe2+-S and Fe3+-S surface species on pyrite fracture-surfaces, and their 3D electronic states, Am. Mineral. 85 (2000) 850–857.

[42] G.K. Reddy, P. Boolchand, P.G. Smirniotis, Unexpected behavior of copper in modified ferrites during high temperature WGS Reaction aspects of Fe3+↔ Fe2+ redox chemistry from mössbauer and XPS studies, J. Phys. Chem. C 116 (2012) 11019–11031.

[43] T. Yamashita, P. Hayes, Analysis of XPS spectra of Fe2+ and Fe3+ ions in oxide materials, Appl. Surf. Sci. 254 (2008) 2441–2449, https://doi.org/10.1016/j.apsusc.2007.09.063.

[44] A. Galtayries, J. Grimblot, Formation and electronic properties of oxide and sulphide films of Co, Ni and Mo studied by XPS, J. Electron Spectros. Relat. Phenomena. 98 (1999) 267–275.

[45] M. Bravo-Sanchez, A. Romero-Galarza, J. Ramírez, A. Gutiérrez-Alejandre, D.A. Solís-Casados, Quantification of the sulfidation extent of Mo in CoMo HDS catalyst through XPS, Appl. Surf. Sci. 493 (2019) 587–592.

[46] M. Zimowska, K. Łątka, D. Mucha, J. Gurgul, L. Matachowski, The continuous conversion of ethanol and water mixtures into hydrogen over FexOy/MoO3 catalytic system—XPS and Mössbauer studies, J. Mol. Catal. Chem. 423 (2016) 92–104.

[47] P.K. Chauhan, S.K. Sharma, H.S. Gadiyar, XPS study of oxides on carbon steel in LiOH at 250° C, Corros. Sci. 21 (1981) 505–515.

[48] M.A. Salim, G.D. Khattak, P.S. Fodor, L.E. Wenger, X-ray photoelectron spectroscopy (XPS) and magnetization studies of iron–vanadium phosphate glasses, J. Non-Cryst. Solids 289 (2001) 185–195.

[49] J.A.R. Guivar, E.A. Sanches, F. Bruns, E. Sadrollahi, M.A. Morales, E.O. López, F.J. Litterst, Vacancy ordered γ-Fe2O3 nanoparticles functionalized with nanohydroxyapatite: XRD, FTIR, TEM, XPS and Mössbauer studies, Appl. Surf. Sci. 389 (2016) 721–734.

[50] N. Parveen, S.A. Ansari, M.O. Ansari, M.H. Cho, Manganese dioxide nanorods intercalated reduced graphene oxide nanocomposite toward high performance electrochemical supercapacitive electrode materials, J. Colloid Interface Sci. 506 (2017) 613–619.

[51] P. Baruah, B.K. Das, M. Bora, B.K. Saikia, D. Mahanta, Hydrothermally prepared sugar-derived carbon spheres for all-solid-state symmetric electrochemical capacitors, Mater. Today Commun. 33 (2022) 104219.

[52] W. Zhao, Y. Wang, A. Wang, J. Qian, W. Zhu, S. Dou, Q. Wang, Q. Zhong, A. Chen, Novel Bi 2 O 2 CO 3/polypyrrole/gC 3 N 4 nanocomposites with efficient photocatalytic and nonlinear optical properties, RSC Adv. 7 (2017) 7658–7670.

[53] J. Ma, A. Guo, S. Wang, S. Man, Y. Zhang, S. Liu, Y. Liu, From the lung to the knee joint: toxicity evaluation of carbon black nanoparticles on macrophages and chondrocytes, J. Hazard Mater. 353 (2018) 329–339.

[54] X. Zhang, Y.-C. Zhang, J.-W. Zhang, B. Zhang, Anchoring ternary CuFePd nanocatalysts on reduced graphene oxide to improve the electrocatalytic activity for the methanol oxidation reaction, RSC Adv. 5 (2015) 101563–101568.

[55] N. Ezzat, M.A. Hefnawy, S.A. Fadlallah, R.M. El-Sherif, S.S. Medany, Synthesis of nickel-sphere coated Ni-Mn layer for efficient electrochemical detection of urea, Sci. Rep. 14 (2024) 14818, https://doi.org/10.1038/s41598-024-64707-z.

[56] M.A. Hefnawy, R. Abdel-Gaber, N. Al-Hoshani, S.S. Medany, Nickel flower/conducting polymer composite for effective ethanol electrooxidation in alkaline medium, Electrocatalysis 15 (2024) 261–271, https://doi.org/10.1007/s12678-024-00868-9.

[57] J.C. Farmer, R.G. Hickman, F.T. Wang, P.R. Lewis, L.J. Summers, Initial study of the complete mediated electrochemical oxidation of ethylene glycol, Lawrence Livermore Laboratory (1991) 1–18.

[58] M.A. Salaev, A.A. Krejker, O. V Magaev, V.S. Malkov, A.S. Knyazev, E.S. Borisova, V.M. Khanaev, O. V Vodyankina, L.N. Kurina, Ethylene glycol oxidation over supported catalyst in tubular reactor, Chem. Eng. J. 172 (2011) 399–409, https://doi.org/10.1016/j.cej.2011.05.079.

[59] S.S. Medany, A. Nafady, R.A. Soomro, M.A. Hefnawy, Construction of chitosan-supported nickel cobaltite composite for efficient electrochemical capacitor and water-splitting applications, Sci. Rep. 14 (2024) 2453, https://doi.org/10.1038/s41598-023-49692-z.

[60] S.S. Medany, M.A. Hefnawy, Nickel–cobalt oxide decorated Chitosan electrocatalyst for ethylene glycol oxidation, Surface. Interfac. (2023) 103077, https://doi.org/10.1016/j.surfin.2023.103077.

[61] M.A. Hefnawy, S.S. Medany, R.M. El-Sherif, N. El-Bagoury, S.A. Fadlallah, High-performance IN738 superalloy derived from turbine blade waste for efficient ethanol, ethylene glycol, and urea electrooxidation, J. Appl. Electrochem. (2023), https://doi.org/10.1007/s10800-023-01862-7.

[62] A. Marchionni, M. Bevilacqua, C. Bianchini, Y. Chen, J. Filippi, P. Fornasiero, A. Lavacchi, H. Miller, L. Wang, F. Vizza, Electrooxidation of ethylene glycol and glycerol on Pd-(Ni-Zn)/C anodes in direct alcohol fuel cells, ChemSusChem 6 (2013) 518–528.

[63] Z. Yu, J. Xu, I. Amorim, Y. Li, L. Liu, Easy preparation of multifunctional ternary PdNiP/C catalysts toward enhanced small organic molecule electro-oxidation and hydrogen evolution reactions, J. Energy Chem. 58 (2021) 256–263, https://doi.org/10.1016/j.jechem.2020.10.016.

[64] T. Ramulifho, K.I. Ozoemena, R.M. Modibedi, C.J. Jafta, M.K. Mathe, Electrocatalytic oxidation of ethylene glycol at palladium-bimetallic nanocatalysts (PdSn and PdNi) supported on sulfonate-functionalised multi-walled carbon nanotubes, J. Electroanal. Chem. 692 (2013) 26–30, https://doi.org/10.1016/j.jelechem.2012.12.010.

[65] M.A. Hefnawy, S.A. Fadlallah, R.M. El-Sherif, S.S. Medany, Systematic DFT studies of CO-Tolerance and CO oxidation on Cu-doped Ni surfaces, J. Mol. Graph. Model. 118 (2023) 108343, https://doi.org/10.1016/j.jmgm.2022.108343.

[66] G. Longatte, O. Buriez, E. Labbé, M. Guille-Collignon, F. Lemaître, Electrochemical behavior of quinones classically used for bioenergetical applications: considerations and insights about the anodic side, Chemelectrochem 11 (2024) e202300542, https://doi.org/10.1002/celc.202300542.

[67] D. Tomczyk, P. Seliger, Modification of glassy carbon electrodes with complexes of manganese(II) with some phenanthroline derivatives immobilized in nafion layer, Int. J. Mol. Sci. 25 (2024), https://doi.org/10.3390/ijms25042348.

[68] J.B. Allen, R.F. Larry, Electrochemical Methods Fundamentals and Applications, John Wiley & Sons, 2001.